IOP Conference Series: Materials Science and Engineering

PAPER • OPEN ACCESS

Numerical modelling of high-power laser spot melting of thin stainless steel

To cite this article: I Bunaziv *et al* 2023 *IOP Conf. Ser.: Mater. Sci. Eng.* **1296** 012012

View the article online for updates and enhancements.

You may also like

- A Study on the Evaluation Tendency of Thermal Sensation in Tropical Region - Targeting short time residents -
K Fukagawa, Y Kurazumi, A Aruninta et al.
- Performance Measurement Of *Mel Frequency Ceptral Coefficient* (MFCC) Method In Learning System Of Al- Qur'an Based In *Nagham* Pattern Recognition
Yesy Afrillia, Herman Mawengkang, Marwan Ramli et al.
- The hydrostatic pressure and magnetic field effect on the diamagnetic susceptibility of a shallow donor in GaAs/AlAs Quantum Box
Y Chrafih, K Rahmani, M Khenfouch et al.

This content was downloaded from IP address 78.91.103.181 on 14/02/2024 at 11:32

IOP Conf. Series: Materials Science and Engineering 1296 (2023) 012012 doi:10.1088/1757-899X/1296/1/012012

Numerical modelling of high-power laser spot melting of thin stainless steel

I Bunaziv[1,*], M H Danielsen[1], M Eriksson[1], X Ma[2], X Ren[2], O E Godinez Brizuela[3], P Skjetne[3]

[1] Materials and Nanotechnology, SINTEF Industry, P.O. Box 4760 Torgarden, NO-7465 Trondheim, Norway

[2] Metal Production and Processing, SINTEF Industry, NO-0314 Oslo, Norway

[3] Process Technology, SINTEF Industry, Trondheim, Norway

*E-mail: ivan.bunaziv@sintef.no

Abstract. Numerical modelling is an important scientific tool in laser materials processing to study different melting, evaporation, and solidification phenomena. It can assist in understanding why certain defects are formed, and thus may provide solution paths for how to decrease certain defects and to increase the quality of a product. Laser spot melting in heat conduction mode represents a simple case and is an excellent first step to build and test solvers prior to moving on to more complicated cases such as laser keyhole welding of thick plates. Modelling of laser spot melting requires only a limited computational domain and allows more complex physics to be added gradually. In this work, a thin 3.0 mm thick stainless steel plate was melted with high-power fiber laser and numerically simulated using a native and custom-build solver based on the VOF method within OpenFOAM. The process was captured with a high-speed imaging camera and simulation results are compared with the experimental results. It was found that temperature-dependent surface tension plays a vital role in controlling melt flow directions within melt pool.

1. Introduction

Laser materials processing plays a significant role in modern industry, encompassing a diverse range of applications and technologies. Its processing range is staggering and is used from nanostructuring for medical applications to thick plate welding or cutting. After many decades of research in laser technology, substantial progress has been made in understanding the interaction between laser-beam and matter. However, there are still many uncertainties, and no universal comprehensive model has been developed to capture all possible phenomena. In processing with high power lasers of metals, there are melting/solidification and evaporation/condensation phenomena with non-linear effects. The latter is among the most challenging phenomenon to model since it includes complex physics and both large spatial and temporal gradients resulting in computationally intensive models. Here we adopt a numerical model based on the finite volume method to study laser spot melting.

Otto et al. **[1]** in 2011 developed an advanced model using OpenFOAM which comes close to representing a universal laser beam model, and is still one of the most notable models. Following publication of their model, numerous other numerical models were published using different software and solution strategies, especially related to laser-powder bed fusion (L-PBF). One of most advanced models was published recently by Gan et al. **[2]** using Ansys Fluent in numerical modelling of keyhole formation in L-PBF where vapour dynamics, ray tracing and complex tangential surface tension forces were included. Recently advanced models for deep laser welding have also been published **[3-6]**.

Content from this work may be used under the terms of the Creative Commons Attribution 3.0 licence. Any further distribution of this work must maintain attribution to the author(s) and the title of the work, journal citation and DOI.
Published under licence by IOP Publishing Ltd

However, few high-quality models are available specifically for laser spot welding. It is simpler since no keyhole is formed but it contains most of the physics involved in both keyhole formation and deep laser welding apart from multiple reflections. Thus, laser spot welding is an excellent starting point for testing numerical models and solution strategies before progressing to the more advanced cases. From an operational point it is of value to be able to predict the transition from a heat conduction dominated operational regime to a keyhole forming regime without having to perform expensive experiments. In heat conduction mode, surface tension plays a key role in predicting melt flow dynamics. The melt pool dynamics is to a large extent driven by a balance of viscous forces, surface tension forces and buoyancy forces. All these forces are sensitive to changes in temperature, resulting in complex temporal and spatial gradients in these forces which drive flow. Typically melt will flow from areas with low surface tension to areas with high surface tension. Such gradients can form e.g., due to compositional differences or temperature gradients. In the latter case the effects are known as thermocapillary effects. Likewise, thermal expansion will induce a change in density resulting in varying buoyancy relative to the average density in the melt. Only a few codes allow for surface tension gradients called as Marangoni forces to be accurately represented in the modelling framework. Some of those that do allow for inclusion of Marangoni forces do so at a large computational cost. Despite a large and growing body of published work, several challenges remain before laser materials processing will have access to efficient and validated general purpose modelling tools. Progress towards this goal is hampered by lack of transparency with regards to details of both modelling and implementation as well as physical data.

OpenFOAM (OF) is an open-source general purpose toolbox for computational fluid dynamics based on the finite volume method. It has a growing community of developers and allows developers to implement and contribute new models and solvers. Due to its open-source nature, running OF is more complicated than running a proprietary GUI driven commercial solver, since it requires general programming skills (in this case the C++ programming language) and Linux OS/WSL system understanding since it cannot be natively run on Windows OS. Therefore, OF has a higher barrier to entry for development compared to most commercial software. OF comes in two distributions, one managed by the ESI-group and one by the OpenFOAM foundation. One of the most promising solvers for laser materials processing is found in the ESI-group's distribution of OF. One of its solvers known as icoReactingMultiphaseInterFoam includes models for phase change and radiative heat transfer, which are key to enabling simulating laser beam energy. It was developed and available in 2018 but is rarely mentioned in the published works. According to the authors' knowledge only a few works have been published which clearly indicated that it was used, e.g., works by Wirth et al. **[7]** and Leung et al. **[8]**. It seems the solver so far has not integrated tangential surface tension forces. The solver was heavily modified in work by Leung et al. where level set method was incorporated, and a laser heat source was added externally. Recently, Flint et al. **[9]** published an alternative model with open-source code where the surface temperature gradient effects in the surface tension has been implemented allowing for accurately accounting for the Marangoni forces. This is achieved by use of an explicit ray tracing model. However, according to the authors' experience, the computational overhead associated with the ray tracing model necessitates the use of high-performance computing to be practical for 3D applications. Moreover, it has limited number of phases involved. The advantages of the native OF solver is that it utilizes the Lagrangian particles for the radiative heat transfer and ray tracing is implicitly implemented which provides faster calculation time. This is discussed by Otto et al. **[10]** where a similar approach was used. Moreover, the multiple reflections can be turned off when they are not required, such as laser spot welding and this will boost the computational speeds immensely. In addition, many phases/species can be included into a model.

In this work, we investigate high power laser beam spot melting on a thin 3.0 mm thick stainless steel plate. Laser beam spot melting is a simple process since it operates in heat conduction mode, however it contains most of the physical phenomena needed to model more complex processes. In heat conduction mode, surface tension plays an important role and capturing the resulting dynamics is one of the main objectives of this work. The process was characterized using a high speed imaging (HSI) camera which allowed direct comparison of the overall dynamics with the numerical modelling. The native OF solver was used and has provided promising results in prediction of melt flows inside the weld pool and partially correlates well with the observed physical phenomena gained from HSI.

However, the solver needs to be modified to include tangential surface tension forces to achieve more realistic melt flow behaviour. The results are compared with works from the literature and critical issues that need to be resolved to improve the solver are elucidated.

2. Methodology

2.1. Materials, equipment and setup parameters

For laser spot welding, a 3.0 mm thick 316L stainless steel was used. In the experiments, a Yb:fiber laser of the IPG Photonics YLS-16000-S2 model was utilized. This continuous wave multi-mode laser operates at a maximum power of 16 kW, with a wavelength of 1070 nm. It features a fiber core diameter of 300 µm and a beam parameter product of 12 mm·mrad. The laser beam exhibited a heat distribution resembling a Gaussian profile. It possessed the following optical parameters: a focal length of 300 mm, with the smallest focused spot size measuring 512 µm in diameter (as measured). Additionally, the Rayleigh length was determined to be 5.6 mm (as measured). To safeguard the spot melt pool from atmospheric conditions, pure argon gas was employed at a flow rate of 10 L/min.

In the initial experiment, a laser power output of 1.0 kW and an irradiation time of 1.5 seconds were utilized. The laser beam was focused at the +60 mm focal point position (*FPP*), resulting in a laser beam spot diameter of 4.1 mm. This configuration enabled the creation of a weld with partial penetration depth (case I). Subsequently, the laser power output was increased to 2.0 kW, leading to a full penetration case, and expanding the model to more complex scenarios (case II). Additionally, a different weld was performed at the +30 mm *FPP* to achieve greater penetration depth and further expand the capabilities of the model (case III).

Spot welds were recorded using a Photron Fastcam Nova S6 type 800K-M-64GB high speed imaging camera at 20 000 frames per second. An illumination diode laser (Cavilux HF 640nm) was used to improve the lighting of the spot welds resulting in improved video quality. The complete melting process was recorded to gain insights into the underlying physics and establish a meaningful correlation with numerical modeling.

2.2. Numerical model description

In this work, both the original and modified *icoReactingMultiphaseInterFoam* was used and tested using OF v2006/v2012/v2106 versions. A few assumptions and simplifications have been made for initial laser spot remelting cases: flow is incompressible and laminar, fluid is Newtonian, and most of thermo-physical parameters are temperature-independent, no multiple reflections are considered/activated, and no evaporation physics was considered. The native solver is designed for N-incompressible phases for transient non-isothermal applications and many phases can be added. The interface tracking was performed using the Volume-of-Fluid (VOF) method which is integrated in OF by default and no modification were used to VOF. Material properties were weighted as a mixture (or volume fraction) of the three primary phases, solid/liquid (stainless steel) metal and gaseous phase (argon). The native solver solves the following equations considering the stated assumptions for mass (equation 1), momentum (equation 2), and energy conservation (equation 3):

$$\frac{\partial \rho}{\partial t} + \nabla \cdot \left(\rho \vec{U}\right) = 0\,, \tag{1}$$

$$\frac{\partial \rho \vec{U}}{\partial t} + \nabla \cdot \left(\rho \vec{U}\vec{U}\right) = -\nabla p + \nabla \cdot \left(\mu \nabla \vec{U}\right) - C_u \left[\frac{(1-f_l)^2}{f_l^3 + 0.001}\right] \vec{U} + \rho g + F_{st}, \tag{2}$$

$$\frac{\partial \left(\rho C_p T\right)}{\partial t} + \nabla \cdot \left(\rho C_p T \vec{U}\right) = \nabla \cdot (k \nabla T) + S_{laser} - h_c\left(T - T_{ref}\right) - \sigma_{sb}\varepsilon_e\left(T^4 - T_{ref}^4\right)\,, \tag{3}$$

Here, the following terms are (every term description from the left to the right consequently): for equation 1: (I) density change with time, and (II) gradient of density change with velocity; for equation 2: (I) density and velocity change with time, (II) divergence of momentum flux, (III) hydrostatic pressure (p) gradient, (IV) viscous stress, (V) the Darcy dampening force for solidification as porous interface

which is modelled through the Voller-Prakash model, (VI) buoyancy force (g is gravitational constant), and (VII) surface tension forces; and for equation 3: (I) change energy per volume with time and (II) the divergence of the thermal energy flux, (III) gradient of heat transfer, (IV) laser heat source, (V) convective losses, and (VI) radiative losses. The nomenclature of symbols is indicated in **Table 1**.

The processing complexity was categorized into three levels, to introduce different physical phenomena gradually for the sake of clarity: (i) Solid body remelting: This level involved only melting and solidification, without any gas phase. Its aim was to establish the Lee constants and provide a quick assessment of the development of the thermal cycle during remelting. (ii) Addition of blanketing gas layer on top: At this level, a gas layer was introduced on top of the solid plate, incorporating surface tension physics. This configuration was typical for partial penetration welding and additive manufacturing scenarios. (iii) Gas layer addition at the bottom: This level featured the inclusion of a gas layer at the bottom, allowing for melt dropout in full penetration cases.

The size of the computational domain was 15×15×(5–7) mm with a base resolution of the computational mesh of 80×80×35 elements. Additional mesh refinement was employed at the centre of the plate. The smallest element size was 0.065 mm and grew to 0.112 mm at the outer edge of the melt pool. To keep the Courant number < 1.0 for fluid velocities in the range of 500–600 mm/s the time step was set to $10e^{-5}$ s. In this work, we consider only modelling which is affordable to run on a standard laptop computer with a few cores (4–6 cores with a frequency of 2.7–4.2 GHz).

The thermos-physical properties used for numerical modelling are shown in **Table 1**.

Table 1. Thermo-physical properties (316L stainless steel) and coefficients used for initial numerical simulations (dimensions provided are aligned with OF conventions). Subscript *s* is for solid (base metal), *l* is for liquid (stainless steel melt), and *g* is for gas (Ar shielding gas).

Density of solid/liquid/gas	$\rho_s/\rho_l/\rho_g$	7900/7500/1.70 kg m^{-3}
Thermal conductivity of solid/liquid/gas	$k_s/k_l/k_g$	18/25/0.018 W m^{-1} K^{-1}
Specific heat of solid/liquid/gas	$C_{ps}/C_{pl}/C_{pg}$	600/775/520 kg^{-1} K^{-1}
Solidus/solidification temperature	T_s	1650 K
Liquidus/melting temperature	T_l	1727 K
Initial surface tension coefficient (liquid/gas)	σ	1.7 N m^{-1}
Latent heat of fusion	H_f	247e3 J kg^{-1}
Absorption coefficient of solid/liquid	a_s/a_l	7e5/6e6 m^{-1}
Dynamic viscosity of liquid/gas	μ_l/μ_g	6.0e-3/2.09e-5 J kg m^{-1} s^{-1}

3. Results and discussion

3.1. Experimental observations

The columns in **Figure 1** show the evolution of the melt pool for the three cases discussed in this section. Laser spot remelting using a 1.0 kW highly defocused laser (+60 mm *FPP*, case I) representing a pure heat conduction welding mode is shown in **Figure 1**a. The depth of the melt pool is shallow and typically exhibits an ellipsoidal shape. This type of melting represents a pure heat conduction welding mode. According to the HSI video, 50 ms is required to form an incipient melt pool. It takes about 500 ms to reach the maximum size of the melt pool. Beyond this time there is a slight increase of the melt pool size between 500 to 1500 ms (the maximum irradiation time). In the beginning of the melt pool formation, there is a clear indication of low outward melt flow velocities. After ~580 ms, a melt stagnation occurs with puls-like melt behaviour with a periodic change in the surface flow between inward and outward flow, with outward melt flow behaviour dominating.

An increase of the laser power to 2.0 kW provided a full penetration of the plate at +60 mm *FPP* (see **Figure 1**b, case II). Due to higher energy input per time, the time scales were shorter. During inception of melting, a slow outward melt flow directions occurred with flow speeds measured in the range of 35–45 mm/s, based on a few floating oxides grains on the surface. With melt stagnation occurring around ~100 ms again followed by puls-like behaviour. The flow then settles into a mode with

strong inward surface flow. Such complex behaviour with flow reversals was also reported by Zhao et al. **[11]**. Moreover, a small vortex formed in the middle of the melt pool that exhibited a counterclockwise rotation. A portion of the melt near the edges continued to have outward melt flows with some periodic pulsing and rotation-like flows around the edges.

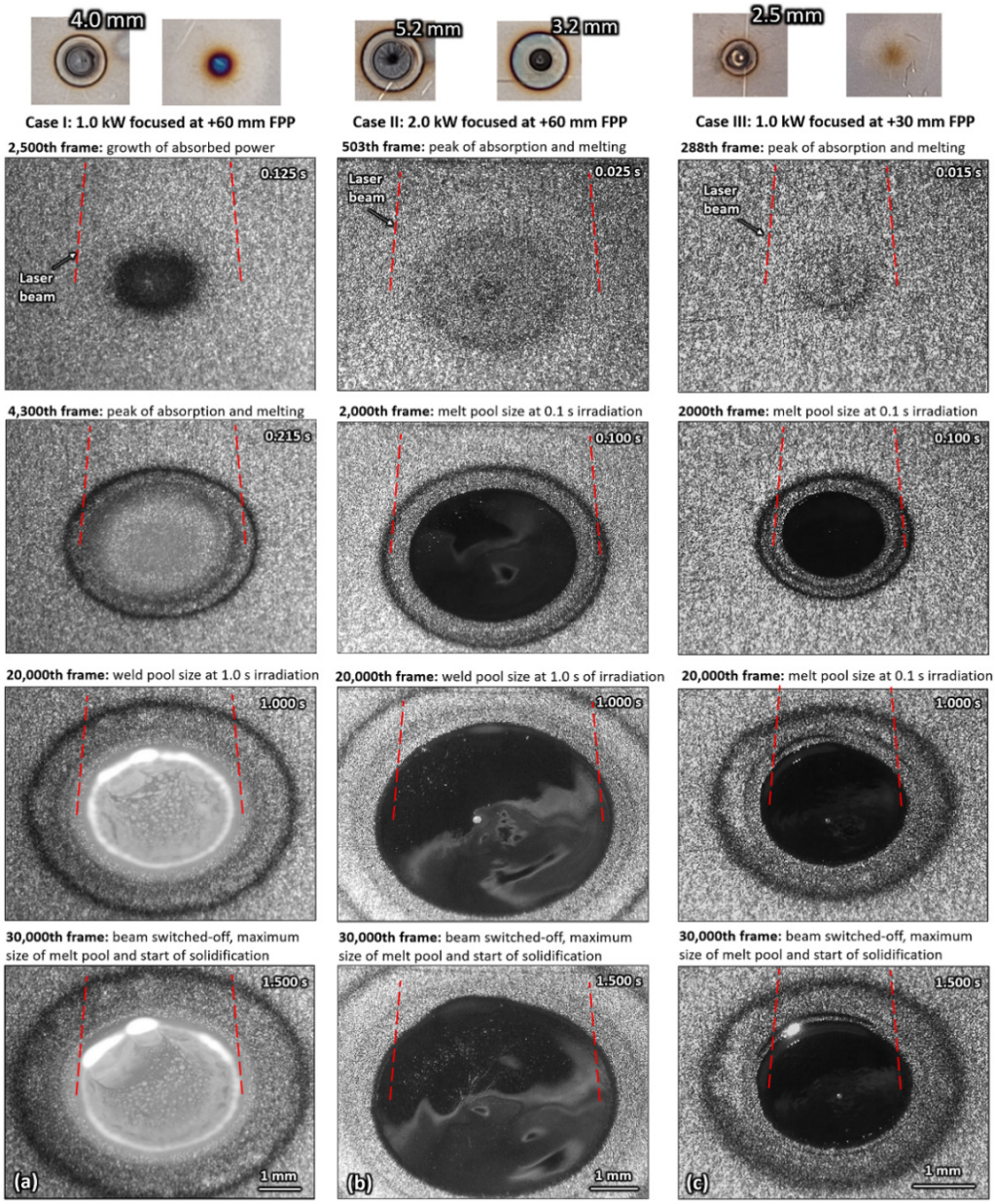

Figure 1. Experimental observation of melt pool formation, growth, and dynamics of melt flows of selected test cases.

A more focused laser beam (+30 *FPP*) with 1.0 kW (see **Figure 1**c, case III), the melt pool dynamics was almost identical to case II. In this case, the vortex is more pronounced and with similar velocity magnitudes of the surface melt flow. Flow reversals occurred slightly earlier at ~60 ms. Cases II and III

were selected for numerical modelling due to their similarity. A complete overview of melt flow behaviour for each case is illustrated in **Figure 2**.

There are a few reasons for the complex melt pool behaviour which is related to surface tension phenomena. In heat conduction laser welding gradients in surface tension dominate the physics resulting in surface flows from areas of low surface tension to areas of high surface tension. It is well known that in pure iron melting by a heat source, only outward melt flows occur (cf. refs in **Figure 3**), and surface tension decreases linearly with temperature, see **Figure 3**a. The temperature is at a maximum at the centre of the melt pool and decreases towards the edges, thus resulting in an outward surface flow. With addition of oxygen or sulphur into the bulk metal, the surface tension no longer exhibits a linear dependence with temperature. Starting from the melting point (for steel) it will first *increase* with increasing temperature until it reaches a maximum after which it will start to *decrease* with a further increase in temperature, cf. **Figure 3**. For sulphur the surface tension goes through a minimum instead of a maximum producing an opposite chain of events **[12]**. In these cases, the initial surface flow will be directed inwards in the pool until the maximum temperature in the pool reaches the temperature corresponding to the maximum value in surface tension. At this point there will be a period where the surface tension gradient is no longer monotonous, and stagnation and pulsing may occur. Once the temperature of the whole melt pool has crossed this maximum temperature the surface melt flow will reverse and flow outwards. If the melt pool becomes larger than the irradiation area of the laser the melt temperature at the edges can drop below the temperature corresponding to the maximum in surface tension and complex edge flows can result. Therefore, based on the performed experimental observations, the surface tension at melting point is high, with no oxygen, and rapidly decreasing with temperature according to the **Figure 3**. In such case, the surface tension temperature gradient **Figure 2**b is negative in the beginning and becomes more positive.

The surface tension temperature gradient causes Marangoni flows and includes the tangential components for the surface tension force that may strongly affect the melt flow behaviour and its direction. Such behaviour can be explained in our case by increase of the oxygen from the surface oxides (the used plates were not cleaned mechanically) present on the plates into the melt pool during the growth of the melt pool. There is also additional explanation of chaotic-like behaviour of the melt pool which can be related to: uneven temperature distribution of melt surface, evaporation, and chemical anisotropy with thermo-physical properties. Due to these phenomena, a realistic spot welding simulation represents a significant challenge in predicting the complex melt flow characteristics and capturing such quasi-stable behaviour which also may require inclusion of turbulent modelling.

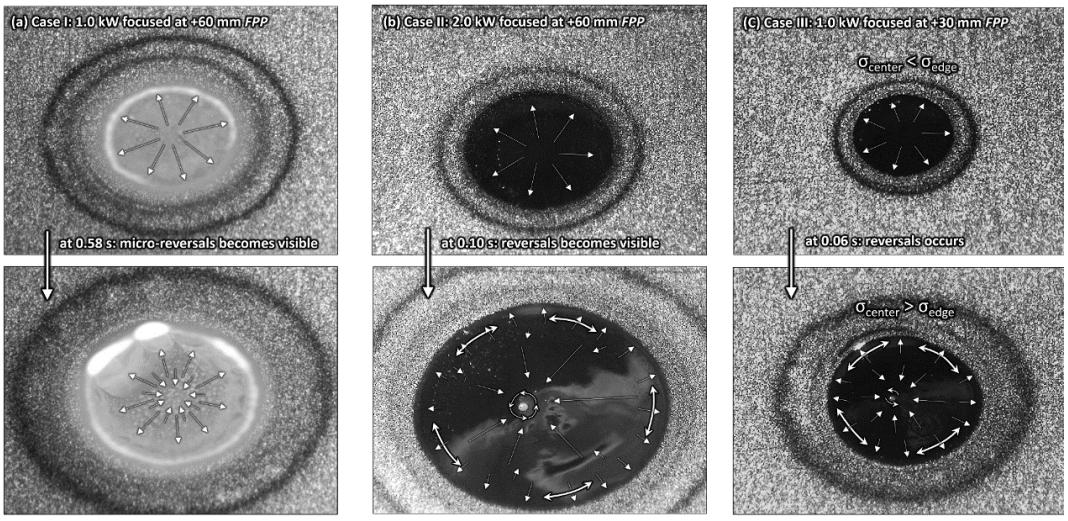

Figure 2. Experimental observation of melt pool formation, growth, and dynamics of melt flows of selected test cases.

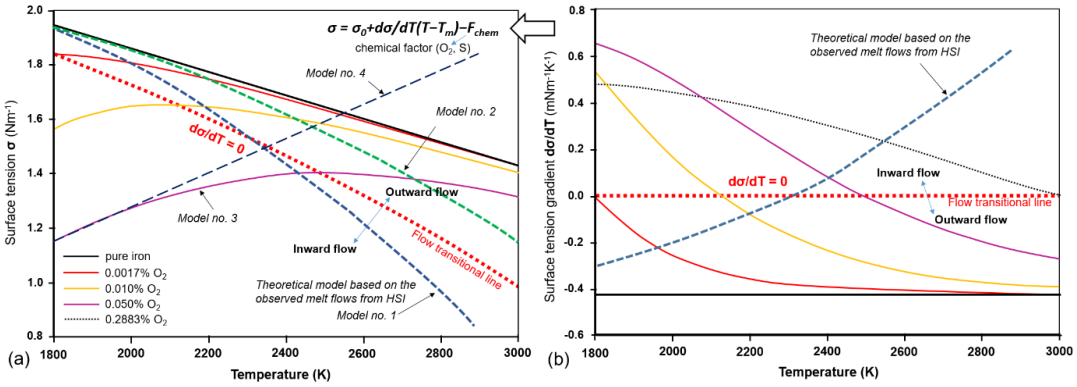

Figure 3. Effect of (a) temperature dependent surface tension and (b) surface tension temperature gradient on melt flow behaviour. Graphs constructed based on **[11]**. Note the curve employed for this work is shown only schematically and approximated with tabulated data in the numerical modelling part.

3.2. Numerical modelling

High speed imaging is an excellent tool to observe dynamic process behaviour. However, it is primarily limited to surface phenomena and internal melt flows cannot be directly observed. Therefore, numerical modelling is a great tool to infer a more complete understanding of the system. Building credible models is a gradual process, starting from first principles accounting for the dominant phenomena in succession. To build credible models requires significant skills both in formulation of the underlying physics and numerical solution of the governing equations. As a first step, we have investigated a simple plate with two phases (solid and liquid) to test the implementation of melting, and to establish approximate melting parameters. In this case, the Lee model of melting was used assuming a porous interface between the two phases. Next, a gas layer was added on top of the plate resulting in a three-phase system. This significantly increased the computational time.

Initially, only the normal component of the surface tension force was included assuming a constant value for the surface tension. From these simulations the melting parameters of the Lee model were tuned to give good agreement with melting times from the experimental part. Good agreement with the fusion zone lines were achieved, cf. **Figure 4**. For case II full penetration occurred with a slight dropout at the root but surface tension prevents formation of a hole, cf. **Figure 4**b.

The melt flows behaviour in all three cases is outward flows. However, the remelt with 1.0 kW at +60 mm *FPP* had a melt flow reversal to inward flow after 800 ms (0.8 s) which occurs only slightly later than experimental observations. At this point such behaviour is unknown but it was not expected to provide flow reversals at constant surface tension. Notably, the numerical model was not able to capture a fully correct melting evolution of the molten pool (considering the liquid fraction of > 0.8) which formed at a slightly later time with delay of 50 ms. Generally, the weld pool evolution times are in good agreement with the experimental observations.

The next step is to include the temperature dependent surface tension which is employed as tabulated data (or polynomial) corresponding to represent three selected cases of surface tension behaviour on temperature. As the prototype, the case with 2.0 kW defocused at +60 mm *FPP* and up to 0.40 s simulation time was considered since the flow reversals occurs early in the beginning and at such time the melt pool is large enough. Furthermore, the bottom gas layer was omitted since no full penetrated is needed for proof of concept and the mesh can be further refined to increase the accuracy.

Initially, two monotonically decreasing models for surface tension as a function of temperature were investigated (Model no. 1 and Model no. 2, cf. **Figure 3**a). Both models started out with a relatively high surface tension of ~1.95 N/m at 1800 K. Model no. 1 exhibited a more rapid decrease in surface tension with temperature compared with Model no. 2. Additionally, both exhibited a linear increase in reduction of surface tension with temperature. Model no. 1 would not converge, and we are still investigating the reasons for the numerical problems seen in these simulations. Model no. 2 had a smaller reduction in surface tension with temperature and would converge. The outward melt from in the

beginning of melting was achieved and only partly reversed into the inward melt flows, see **Figure 5**a. Therefore, the proposed model only partially in agreement with the experimental observations.

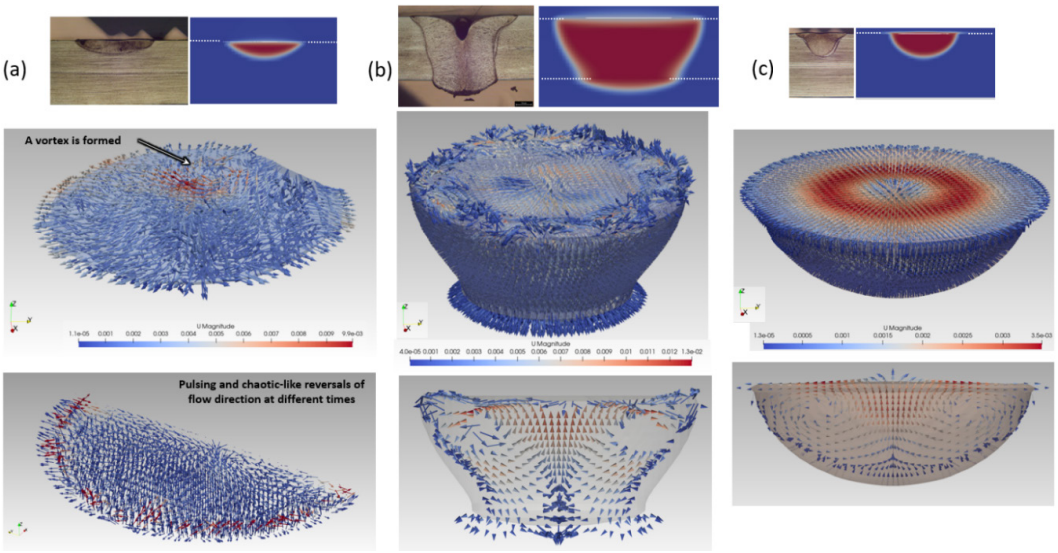

Figure 4. Numerical modelling results of the selected cases with constant or temperature independent surface tension. Comparison of fusion zone geometry and melt flows in case of (a) defocused 1.0 kW laser at +60 mm *FPP* at different timings, (b) defocused 2.0 kW laser at +60 mm *FPP* at 1.5 s (end of welding time), and (c) defocused 1.0 kW at +30 mm *FPP* at 1.5 s (end of welding time).

The next model, Model no. 3 cf. **Figure 3**, represented a steady increase of the surface tension with temperature and a slight decrease after 2400 K. The inward melt flow was achieved at start of melting and transited to outward flow in a short time (see **Figure 5**b) which is in a good agreement with the theoretical assumptions (see **Figure 3**) and the model responded correctly to the temperature dependency of the surface tension coefficient. However, no vortex was formed in the centre and flow behaviour was not realistic exhibiting random waviness upon enlargement of the melt pool. The final surface tension model investigated, Model no. 4 cf. **Figure 3**, exhibited a gradual (linear) increase in surface tension with temperature. Unlike Model no. 3, it only exhibited inward flow in the main melt pool. Close to the edges a thin annular region exhibited outward flow accompanied by small tangential flows creating a number of eddies along the edge. A large vortex was gradually formed at the centre of the melt pool which represent mostly inward melt flows as shown in **Figure 5**c. This is in a good agreement with the experimental observations except that the melt flow did not exhibit flow reversal at the start of melting. Intermittently, smaller vortices were formed around the large central vortex having short lifetimes dissipating rapidly. The central vortex became quasi-stable state after > 0.30 s. The melt flow velocities increased significantly compared to the cases with constant surface tension (see **Figure 4**) and were at a maximum at the centre of the melt pool.

According to theoretical assumptions, more oxides enter the weld pool as it grows, hence the surface tension should increase with temperature. To exhibit flow reversal the surface tension needs to pass through a maximum as temperature increases. This could result from increasing in oxides concentration but warrants further investigation and access to data for stainless steel as **Figure 3** is only valid for iron systems. Hence, some discrepancy between theoretical considerations based on **Figure 3** and our experimental observations of stainless steel should be expected.

Addition of the tangential component of the surface tension force was included using the code provided by Wirth et al. **[7]**. However, no difference was found as shown in **Figure 5**d. It may be related to: (*i*) rough mesh size which is unable to properly capture tangential surface tensions; (*ii*) for the presented case using higher laser power than for typical L-PBF, these forces may have a low effect;

and/or (*iii*) the native solver somehow derives the tangential surface component by itself using the temperature-dependent surface tension which cannot be confirmed at this point. A further mesh refinement yielded similar results, **Figure 5**e-f, for both unmodified and modified solvers. In general, the VOF method struggles to capture effects such as the Marangoni forces due to the dissipative nature of the surface reconstruction. Based on the provided modelling results, the significance of the tangential surface tension component is low. A non-monotonic temperature dependent surface tension which included only the normal component was all that was needed to capture flow reversal in the melt pool as it heated up. Unfortunately, the proposed models were not able to fully coupe with all the details observed experimentally using HSI. The future work will employ more refined mesh models which will require more powerful computational workstations for higher efficiency.

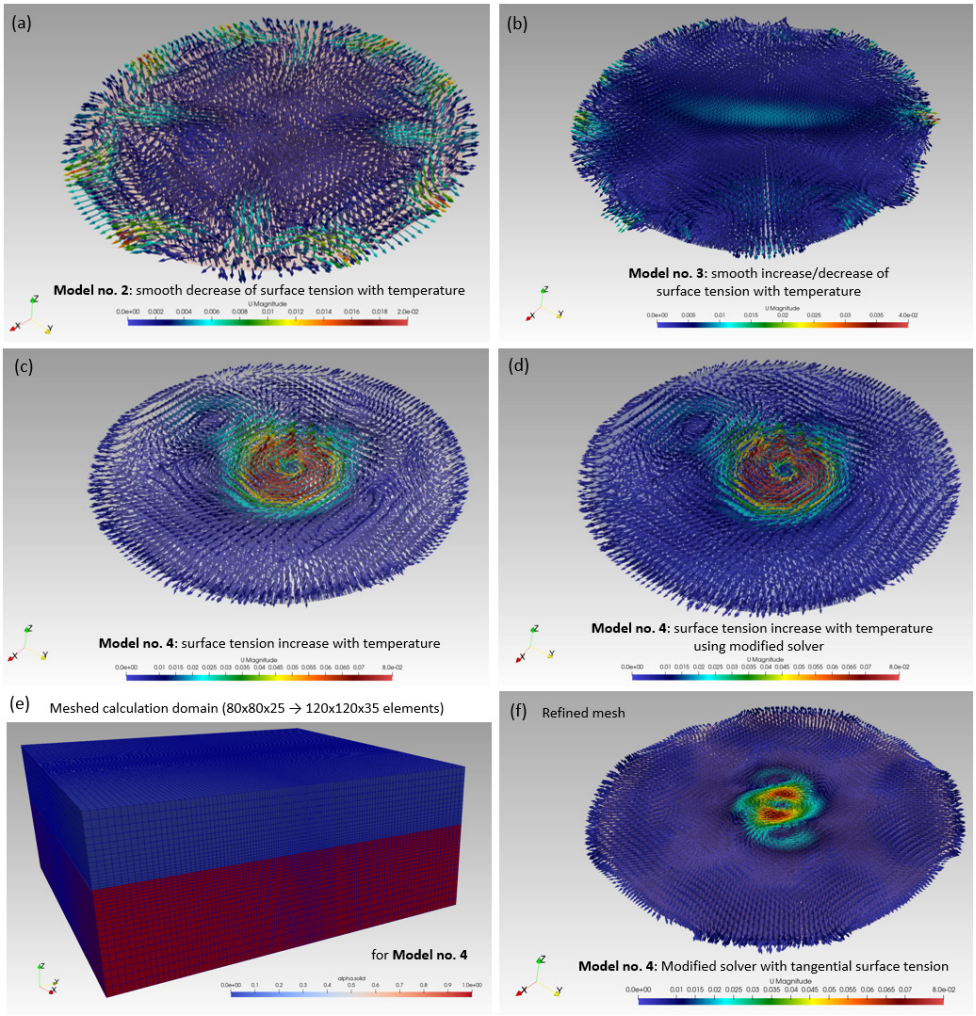

Figure 5. Numerical modelling results of the selected case (2.0 kW focused at +60 mm *FPP*) using different temperature dependent surface tension models at 0.40 seconds.

In this work it has been demonstrated that the identification of the melt flow directions and their magnitudes is challenging to estimate based on the experimental observations. The HSI equipment is unable to show the melt characteristics inside the melt pool, thus it is limited to the observations on the surface. In fact, very accurate measurement and numerical estimated melt flow velocities are not required, hence only a general understanding of the flow patterns is needed and is enough to understand

the process behaviour with possible formation of weld defects (or penetration depth) which is the main purpose of the numerical modelling and experimental observations. In general, numerical modelling is a complex procedure and to achieve similar results is challenging since precise thermo-physical parameters of the base metal must be known. Moreover, they are temperature dependent. Absorption coefficients are difficult to estimate and cannot be readily measured which also depends on the temperature and phase of the absorbing media. The relationship of temperature-dependent surface tension and flow direction is difficult to measure practically and rarely provided in the literature for a certain alloy system. Other thermo-physical parameters may also affect the fluid flow such as temperature-dependent viscosity and vaporisation which were not tested here. A high-fidelity model may reduce the knowledge gap and explain the melt flow behaviour more correctly.

4. Summary and conclusions

The experimental data and the numerical modelling showed a good agreement with regard to weld pool growth and the general nature of the melt flows. The native OpenFOAM solver was tested for the simplest case at low power heat conduction laser spot welding. A successful implementation of the temperature-dependent surface tension was performed with testing of different models to control directions of the melt flows. The normal surface tension component was sufficient to model and control the flow reversals. Therefore, the selected solver may provide a reliable and realistic behaviour of the melt pool. At this point it is not clear if the tangential surface tension component is absent in the native solver or should be introduced and tested properly for the future works.

Acknowledgments

The experimental work was conducted in MANULAB (Norwegian Manufacturing Research Laboratory) infrastructure, funded by the Norwegian Research Council (Grant No: 269898).

References

[1] Otto A, Schmidt M 2010 Towards a universal numerical simulation model for laser material processing. *Phys. Procedia* **5** 35-46
[2] Gan Z, Kafka O L, Parab N, Zhao C, Fang L, Heinonen O, Sun T, Liu W K 2021 Universal scaling laws of keyhole stability and porosity in 3D printing of metals. *Nat. Commun* **12**(1) 2379
[3] Sun Y, Li L, Hao Y, Lin S, Tang X, Lu F 2022 Numerical modeling on formation of periodic chain-like pores in high power laser welding of thick steel plate. *J. Mater. Process. Technol* **306** 117638
[4] Wang Y, Jiang P, Geng S, Xu B, Zhao J 2022 Influence of the wrinkle surface structures on the vapor flow and keyhole stability in 20 kW high power laser welding. *Int. J. Heat Mass Transf.* **193** 122958
[5] Artinov A, Meng X, Bachmann M, Rethmeier M 2022 Study on the transition behavior of the bulging effect during deep penetration laser beam welding. *Int. J. Heat Mass Transf.* **184** 122171
[6] Geng S, Yang W, Jiang P, Han C, Ren L 2022 Numerical study of keyhole dynamics and porosity formation during high‐power oscillating laser welding of medium‐thick aluminum alloy plates. *Int. J. Heat Mass Transf.* **194** 123084
[7] Wirth F, Tonn T, Schöberl M, Hermann S, Birkhofer H, Ploshikhin V 2022 Implementation of the Marangoni effect in an open-source software environment and the influence of surface tension modeling in the mushy region in laser powder bed fusion (LPBF). *Model. Simul. Mater. Sci. Eng.* **30**(3) 034001
[8] Leung C L A, Luczyniec D, Guo E, Marussi S, Atwood R C, Meisnar M, Saunders B, Lee P D 2022 Quantification of Interdependent Dynamics during Laser Additive Manufacturing Using X-Ray Imaging Informed Multi-Physics and Multiphase Simulation. *Adv. Sci.* **9**(36) 2203546
[9] Flint T F, Robson J D, Parivendhan G, Cardiff P 2023 laserbeamFoam: Laser ray-tracing and thermally induced state transition simulation toolkit. *SoftwareX* **21** 101299
[10] Otto A, Vázquez R G 2018 Fluid dynamical simulation of high speed micro welding. *J. Laser Appl.* **30**(3) 032411
[11] Zhao C X, Kwakernaak C, Pan Y, Richardson I M, Saldi Z, Kenjeres S, Kleijn C R 2010 The effect of oxygen on transitional Marangoni flow in laser spot welding. *Acta Mater.* **58**(19) 6345-57
[12] Pitscheneder W, DebRoy T, Mundra K, Ebner R 1996 Role of Sulfur and Processing Variables on the Temporal Evolution of Weld Pool Geometry during Multikilowatt Laser Beam Welding of Steels. *Weld J.* **75** 71-80